Volume 14
Number 16
28 April 2022
Pages 1555–1656

Analytical Methods

rsc.li/methods

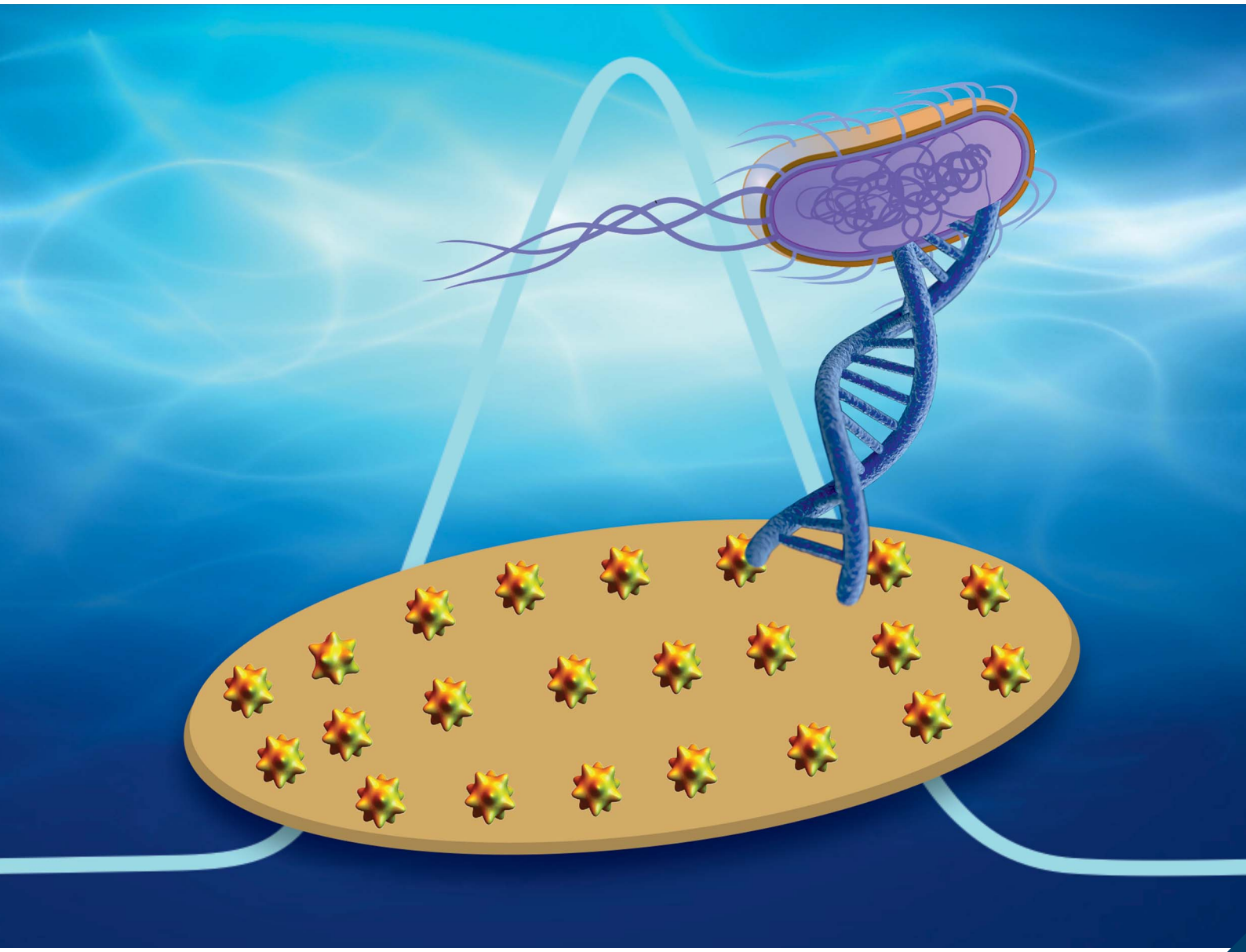

ISSN 1759-9679

ROYAL SOCIETY OF CHEMISTRY

PAPER
Nasrin Razmi *et al.*
Electrochemical genosensor based on gold nanostars for the detection of *Escherichia coli* O157:H7 DNA

Indexed in Medline!

Analytical Methods

ROYAL SOCIETY OF CHEMISTRY

PAPER

View Article Online
View Journal | View Issue

Cite this: *Anal. Methods*, 2022, **14**, 1562

Electrochemical genosensor based on gold nanostars for the detection of *Escherichia coli* O157:H7 DNA†

Nasrin Razmi, *[a] Mohammad Hasanzadeh,[b] Magnus Willander*[a] and Omer Nur [a]

Escherichia coli O157:H7 (*E. coli* O157:H7) is an enterohemorrhagic *E. coli* (EHEC), which has been issued as a major threat to public health worldwide due to fatal contamination of water and food. Thus, its rapid and accurate detection has tremendous importance in environmental monitoring and human health. In this regard, we report a simple and sensitive electrochemical DNA biosensor by targeting Z3276 as a genetic marker in river water. The surface of the designed gold electrode was functionalized with gold nanostars and an aminated specific sensing probe of *E. coli* O157:H7 to fabricate the genosensor. Cyclic voltammetry (CV) and square wave voltammetry (SWV) techniques were applied for electrochemical characterization and detection. The synthesized gold nanostars were characterized using different characterization techniques. The fabricated DNA-based sensor exhibited a high selective ability for one, two, and three-base mismatched sequences. Regeneration, stability, selectivity, and kinetics of the bioassay were investigated. Under optimal conditions, the fabricated genosensor exhibited a linear response range of 10^{-5} to 10^{-17} μM in the standard sample and 7.3 to 1×10^{-17} μM in water samples with a low limit of quantification of 0.01 zM in water samples. The detection strategy based on silver plated gold nanostars and DNA hybridization improved the sensitivity and specificity of the assay for *E. coli* O157:H7 detection in real water samples without filtration. The detection assay has the advantages of high selectivity, sensitivity, low amounts of reagents, short analysis time, commercialization, and potential application for the determination of other pathogenic bacteria.

Received 12th January 2022
Accepted 9th March 2022

DOI: 10.1039/d2ay00056c

rsc.li/methods

Introduction

E. coli O157:H7 as a subset of enterohemorrhagic *E. coli* is an important waterborne and foodborne pathogen responsible for numerous worldwide outbreaks of kidney failure, stomach cramps, diarrhea, life-threatening hemolytic uremic syndrome (HUS), and other illnesses and even death in humans.[1–3] Since its initial discovery in 1982, *E. coli* O157:H7 has become one of the most infective and health-threatening foodborne and waterborne pathogens, inflicting a large challenge in terms of healthcare cost.[4,5] *E. coli* O157:H7 can be passed to people primarily through contaminated food or water consumption.[6] Conventional standard methods for the accurate detection of *E. coli* O157:H7 rely on microbiological and culture-based methods, which are labor-intensive, tedious, and time-consuming.[7] Although the polymerase chain reaction (PCR) offers greater sensitivity and specificity, it is susceptible to inhibition by certain inhibitory components of the sample.[8] Moreover, it has limitations of sample cross contamination risk, lengthy experimental procedure, high cost and the requirement of skilled technical personnel.[2] Enzyme-linked immunosorbent assay (ELISA) is an immunological technique designed for screening either antibodies or antigens in a given sample.[9–12] Despite a few advantages, ELISA has certain limitations such as

[a]*Physics and Electronics, Department of Science and Technology, Linköping University, SE-601 74 Norrköping, Sweden. E-mail: Nasrin.razmi@liu.se; magnus.willander@liu.se; Tel: +46 11 36 34 72*

[b]*Pharmaceutical Analysis Research Center, Tabriz University of Medical Sciences, Tabriz 51664, Iran*

† Electronic supplementary information (ESI) available: Fig. S1: TEM images of AuNSs. Fig. S2: TEM images of AuNSs in atomic scale resolution. Fig. S3: EDX analysis of (A) AuNSs modified electrode (B) AuNSs-pDNA modified electrode, (C) AuNSs-pDNA-cDNA modified electrode. Fig. S4: Size distribution analysis of AuNSs by DLS. Fig. S5: Zeta potential analysis of AuNSs. Fig. S6: (A) SWVs of the fabricated genosensor after hybridization in different incubation time of tDNA (10, 30 and 40 min). Supporting electrolyte is 0.01 M $(Fe(CN)_6)^{3/4}$–KCl). Step size is 10 mV. (B) Histogram of cDNA incubation time. Fig. S7: (A) SWVs (E step = 0.01 V, amplitude 0.1 V, frequency 1.0 Hz) of the DNA sensor after hybridization by 5 microliter of 7.3 μM cDNA, 7.3 μM 1-mismatch DNA, 7.3 μM 2-mismatch DNA and 7.3 μM 3-mismatch DNA in 0.01 M $(Fe(CN)_6)^{3/4}$–KCl) (incubation time 30 min at room temperature). (B) Histogram of the selectivity study. Fig. S8: (A) Dependency of anodic/cathodic peak currents *vs.* potential sweep rate. (B) Dependency of anodic/cathodic peak currents *vs.* square root of potential sweep rate. (C) Dependency of $\ln I_p$ *vs.* $\ln \nu$. (D) Dependency of E_p *vs.* $\ln \nu$. (E) Dependency of I_p: I_{Pc}. Fig. S9: Regeneration study: (1) SWV signal of Au-GNSs-pDNA-MCE-TB-tDNA. (2) SWV signal of Au-GNSs-pDNA-MCE-TB-tDNA after keeping at 60 °C for 3 min and after re-hybridization. Fig. S10: Interday stability of the Au/GNSs/pDNA electrode. See DOI: 10.1039/d2ay00056c

requiring well-trained staff, high cost, lengthy procedure steps and long analysis time.[3,6] Therefore, there is a necessity to develop a sensitive, selective, rapid, and simple detection method of *E. coli* O157:H7 for application in the food industry, environmental monitoring, and clinical diagnosis.

In recent years, biosensors have become an ideal option to overcome the shortcomings in the field of screening pathogens, attributed to their cost-efficiency, simplicity, sensitivity, selectivity, portability, fast response time and real-time measurement.[13,14] A biosensor is essentially composed of a bioreceptor and a transducer to detect a target analyte by producing a measurable signal.[15] Among a variety of transducers, electrochemical biosensors emerge as a powerful tool for pathogenic bacteria detection. Recently, electrochemical deoxyribonucleic acid (DNA) biosensors based on nucleic acid hybridization have gained considerable attention for the detection of *E. coli* O157:H7 owing to their high sensitivity, selectivity, simplicity, and short reaction time. DNA hybridization event is the basic principle of nucleic acid biosensors.[1,16] Genosensors depend on the specificities and strengths of the ribbon interactions that produce the double helix, in which adenine nucleotide with thymine and cytosine with guanine bind specifically.[17] Based on DNA hybridization, single-stranded DNA (ssDNA) probe complementary to a DNA sequence of interest is immobilized on the sensing substrate in order to recognize the targeted DNA. Next, the DNA hybridization is detected by redox activity of the electroactive labels or changes in the electrochemical parameters and then convert it to analytical signal.[18,19] The association of intrinsic advantages of electrochemical biosensors and the high-selective nature of the DNA, coupled with nanoscale materials, has aroused great attention, and a few sensitive and innovative approaches for *E. coli* O157:H7 determination in different fields such as food safety, biomedical and environmental monitoring have been demonstrated.[6,16,20]

In genosensors, nanomaterials can be applied as tracers, signaling elements, and catalysts of the electron transfer process to improve the analytical performance. Nanoparticles in genosensors allow large loadings of DNA probes for immobilization without changing their bioactivity.[21] The unique characteristics of nanoparticles lead to their integration in DNA sensors to obtain improved performance in terms of selectivity and sensitivity. Among the different nanostructured materials, gold nanoparticles (AuNPs) have been widely employed to enhance the analytical performance of electrochemical biosensors due to their distinct electronic, electrochemical, and interface-dominated properties, biocompatibility, large surface area to volume ratio, simple synthesis, stability, and ability to conjugate with biomolecules.[22] Gold nanoparticles can decrease the overpotentials of electrochemical reactions to sustain the reversibility of redox reactions. Gold nanoparticles allow the electrochemical sensing without electron transfer mediators by allowing direct electron transfer of redox proteins with bulk materials of electrode.[23] Integration of gold nanoparticles with DNA based sensors could improve the immobilization of oligonucleotides on the surface of the electrode and signal amplification. By engineering the size and shape of gold nanoparticles, one can improve the conductivity, large surface area for immobilization of biomolecules, and the capacity to offer a natural environment for biomolecules.[21]

The most important factor of designing a DNA based electrochemical biosensor for identifying bacterial pathogens is the high specificity of the DNA probe. The open reading frame (ORF) Z3276 has been initially reported for *E. coli* O157:H7.[24] Blast analysis of the NCBI database indicated that the fimbrial protein encoding Z3276 is a stable and specific genetic marker for *E. coli* O157:H7 identification. The specificity of Z3276 for the detection of *E. coli* O157:H7 strains has been previously confirmed by other scientific studies.[25,26] In this regard, we report a new sensitive, selective, and rapid electrochemical DNA sensor targeting the Z3276 gene, using a 90 nm gold coated glass slide functionalized with gold nanostars for larger surface area and rapid electrochemical signal as depicted in Fig. 1. The specific DNA probe immobilized onto the functionalized gold electrode and mercaptoethanol are used to block the active sites to decrease non-specific adsorption. Toluidine blue (TB) is used to label the DNA probe, and *E. coli* O157:H7 DNA target is quantified by square wave voltammetry technique (SWV). The synergetic effect of SWV and the efficiency of the engineered DNA sensor led to the 0.01 zM low limit of *E. coli* O157:H7 quantification, confirming its potential application in food safety and environmental monitoring.

Materials and methods

Apparatus

Electrochemical characterization, kinetic study, and two samples of electrochemical responses in standard and water samples were performed with Gamry Potentiostat Interface 1010B (manufactured by Gamry Instruments) controlled by the Framework software. Optimization of the DNA hybridization, regeneration study, stability study, selectivity, and one sample of electrochemical response of the genosensor were performed by PalmSens system PS4·F1.05 (Palm instruments, Utrecht, The

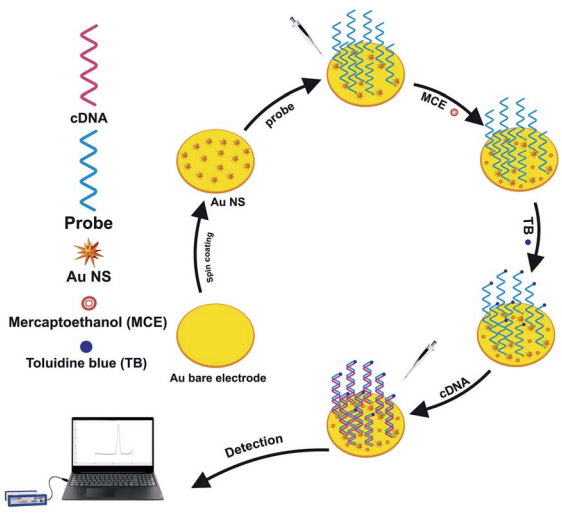

Fig. 1 Graphical illustration of the DNA biosensor for the detection of the *E. coli* O157:H7 pathogen.

Netherlands) operated with PSTrace software. The working electrode (r = 1 mm) was prepared by deposition of a 90 nm-thick gold layer on the glass substrate by a vacuum evaporation system (Balzers BA 510) using a designed stencil shadow mask (from Beta LAYOUT GmbH). Platinum wire auxiliary electrode 50HX15 0.6/250 mm (from Redoxme AB) and silver/silver chloride (Ag/AgCl) reference electrode (from Redoxme AB) were used to complete the three-electrode setup. All electrodes were placed on a Bottom Magnetic Electrochemical Cell (from Redoxme AB), on which the working electrode was loaded from the bottom *via* magnetic mount, while reference and counter electrodes were mounted on top. For the square-wave-voltammetry measurements, a frequency of 1.0 Hz, amplitude of 0.1 V and step size of 10 mV were applied. All electrochemical tests were performed in a supporting electrolyte of 0.01 M ferro-ferricyanide containing 0.01 M potassium chloride. The characterization and chemical compositions of the synthesized gold nanostars were performed with field emission scanning electron microscopy (Zeiss Sigma 500 Gemini FE-SEM) equipped with an EDS detector. Further exploration of gold nanostars was done at the atomic scale using high angle annular dark field scanning transmission electron microscopy (HAADF-STEM) imaging and energy-dispersive X-ray (EDX) analysis. Characterization was performed using the Linköping double Cs corrected FEI Titan^3 60-300 operating at 300 kV. HAADF-STEM imaging was performed using a 21.5 mrad convergence semi-angle, which provided sub-Ångstrom resolution probes with ~60 pA beam current. The HAADF-STEM images were recorded using an angular detection range of 46–200 mrad. EDX maps are obtained using a SuperX detector embedded in the FEI instrument. DLS (dynamic light scattering) and ZP (zeta potential) measurements were carried out *via* Zetasizer Nano ZS90 by Malvern. Studies of the absorption spectra were performed using PerkinElmer Lambda 900 spectrophotometer.

Chemicals and reagents

All the oligonucleotide sequences described in Table 1 were produced by Integrated DNA Technologies (Belgium). Au 99.99% was obtained from Nordic High Vacuum AB (Sweden). All the chemicals used in this work were purchased from Sigma Aldrich, including the gold(III) chloride solution ($HAuCl_4$), silver nitrate ($AgNO_3$), sodium borohydride ($NaBH_4$), sodium citrate ($C_6H_5Na_3O_7$), L-ascorbic acid ($C_6H_8O_6$), (1-hexadecyl)trimethylammonium bromide ($CH_3(CH_2)_{15}N(CH_3)_3Br$), mercaptoethanol ($HSCH_2CH_2OH$), toluidine blue ($C_{15}H_{16}ClN_3S$), trizma hydrochloride ($C_4H_{11}NO_3 \cdot HCl$), potassium hexacyanoferrate(II) trihydrate ($C_6FeK_4N_6 \cdot 3H_2O$), potassium hexacyanoferrate(III) ($C_6FeK_3N_6$), and potassium chloride (KCl). Deionized (DI) water was used throughout this experiment.

Synthesis of gold nanostars

Seed-mediated growth method due to the ease of controlling the size and shape of the formed nanoparticles through the adaption of nucleation and growth conditions was used for the synthesis of temperature and time dependent gold nanostars in three main steps as follow.[27,28]

Preparation of silver seeds. In the first step, 0.25 mL of sodium citrate (5 mM) was added to 10 mL of silver nitrate solution (0.25 mM) while stirring. Next, 0.4 mL of the prepared cooled solution of sodium borohydride (40 mM) was added quickly to the solution and stirred for 5 min. The prepared silver seed solution was kept in a dark place and at room temperature without a lid for 2 h.

Preparation of the growth solution. In this step, 20 mL of completely dissolved CTAB solution (50 mM) on a stirring hot plate (30 °C) was prepared. Next, the hotplate was turned off, and 0.06 mL of silver nitrate solution (16.3 mM) was added. After 60 s, a calculated amount of the gold chloride solution was added and stirred for 60 s. Then, 0.1 mL of L-ascorbic acid (80 mM) was added, which made the solution colorless. In 20 s, 0.05 mL of silver seeds were added, and after 60 min of stirring, the final brown growth solution was kept isolated from the dark for 24 h.

Washing step. After 24 h, the solution was heated at 30 °C to dissolve the CTAB crystals. The solution was centrifuged for 12 min at 2500 rpm and 20 min at 3000 rpm. The concentrated nanoparticles in a centrifuge tube were used for characterization and experiment.

Preparation of the genosensor

Fig. 1 schematizes the stepwise fabrication of the genosensor for detection of *E. coli* O157:H7. Initially, glass slides were effectively cleaned by ultrasonically treating in acetone, ethanol, and DI water and drying with nitrogen. In the next step, the Au electrode (r = 1 mm) was prepared by deposition of 10 nm of chromium and a 90 nm-thick gold layer on the glass substrate by vacuum evaporation system using a designed stencil shadow mask (Fig. 2). As shown in Fig. 2, a circular-shaped Au electrode (r = 1 mm) was used as the working electrode in the whole experiment, and one of the connectors has been used to connect the working electrode to the system using a Bottom Magnetic

Table 1 Oligonucleotide sequences

Description	Purification	Concentration (μM)	Sequence
Probe	HPLC	8.33	5AmMC6/TA GCC TTA CCG CTG ACC CAT TGT T
Complementary target	PAGE	7.3	AAC AAT GGG TCA GCG GTA AGG CTA
Single base mismatch target	PAGE	7.34	AAC GAT GGG TCA GCG GTA AGG CTA
Double bases mismatch target	PAGE	7.23	AAC AAT GAG TCA TCG GTA AGG CTA
Three bases mismatch target	PAGE	7.43	AAC AGT GGA TCC GCG GTA AGG CTA

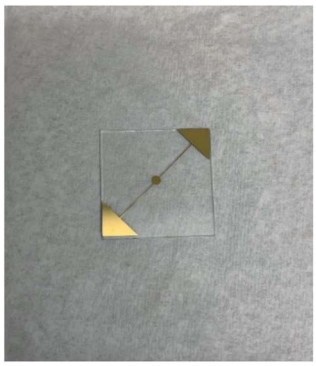

Fig. 2 Au electrode.

Electrochemical Cell, on which the target area of the working electrode was loaded from the bottom *via* a magnetic mount. Thereafter, the previously mentioned cleaning steps were repeated to clean the surface of the prepared Au electrodes. Then, gold nanostars were deposited on the electrode by a spin-coater with a low spin speed of 200 and then 500 rpm. The process was repeated 2 times, and the confirmation of the deposition was investigated by CV technique, microscopy methods, and characterization techniques. Next, the electrochemical behavior of the electrodes was evaluated by the CV technique. Since gold has an affinity to amine functional groups,[29] 5 microliters of 8.38 μM aminated probe oligos in 10 mM Tris–HCl/0.1 mM EDTA buffer with a pH of 8.0 was drop-casted on the gold nanostar-modified Au electrode and incubated for 2 h at 4 °C. Next, the DNA-modified Au/GNSs was further treated with 5 microliters of mercaptoethanol for 30 min at room temperature to obtain a well aligned probe oligo monolayer and block the remaining unattached gold sites. Subsequently, 5 microliters of TB containing Tris–HCl was drop-casted on the genosensor for 15 min at room temperature. TB is a basic thiazine metachromatic dye having a high tendency for nucleic acids.[30] Thus, due to the uptake of DNAs, TB was used to mark the probe oligo. The hybridization process was performed by drop-casting Tris–HCl/0.1 mM EDTA containing various concentrations of target oligo for 30 min at room temperature. The same hybridization process was performed for water samples with different concentrations of target oligo.

Results and discussion

Characterization of nanoparticles

Characteristics of the engineered nanomaterials within 1–100 nm size range differ from their smaller atoms and bulk counterparts. The physicochemical properties significantly rely on the shape, size, size distribution, morphology, and surface charge, and in the presence of certain chemicals, these properties could be modified. A large surface area is of utmost importance, which contributes to the wide application of nanomaterials in biosensors. In the present study, sodium borohydride, sodium citrate, and hexadecyl trimethylammonium bromide (CTAB) were used as the reducing, capping agent, and stabilizer, respectively. It should be noted that the temperature, pH, and the use of certain chemicals in the growth solution influence the growth and finally the size and shapes of the nanoparticles. The method used ascorbic acid acting as a reducing agent and $AgNO_3$ to provide Ag ions as a catalyst. It seems that the anisotropic growth of the nanoparticles was upon the addition of CTAB, and the process of growth was gradual *via* a kinetically controlled mechanism.

The morphology of the gold nanostars was observed by SEM (Fig. 3) and TEM (Fig. 4 and S1; see online ESI†). The result shows a successfully coated star shaped structure, which comprises the building units of about 10 nm nanoparticles. The star shaped structure led to a greater surface area, which provided an excellent scaffold for the high loading of probe oligos. SEM also was used to characterize the genosensor before hybridization and after hybridization of the target sequences with probe sequences (Fig. 3). It is shown that the probe sequences were successfully attached to the gold nanostars (Fig. 3(b)). Fig. 3(c) shows the successful hybridization of the target oligos with probe oligo (Fig. S2; see online ESI†) and shows no defects and dislocations in the structure of gold nanostars at atomic scale resolution by TEM. Fig. 4 indicates the elements of structural construction of Au, Ag and their arrangement of an entire nano-star. The result shows that there is a very thin coating of Ag on the shell of the structure (Fig. S3; see online ESI†). Depicts the EDX analysis of a further study of the composition of the genosensor in each step of fabrication. As presented in (Fig. S3; see online ESI†), a strong sharp signal

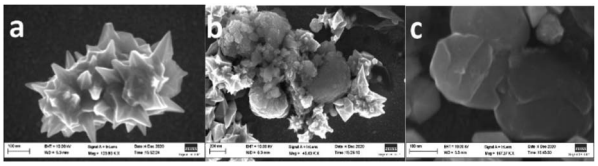

Fig. 3 SEM images of (a) AuNSs, (b) AuNSs-pDNA, and (c) AuNSs-pDNA-cDNA.

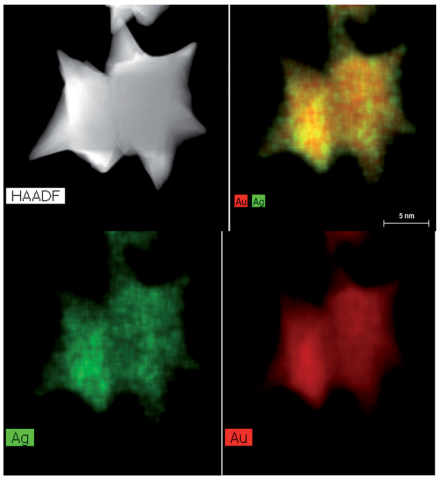

Fig. 4 EDX analysis of AuNSs.

of Au is present in all spectra. Si signal belongs to the substrate. Irrelevant small signals of Fe might correspond to a residue from the environment (Fig. S4; see online ESI†). Depicts the size distribution analysis. Positive zeta potential of 44.5 mV indicates the positive surface charge of AuNSs (Fig. S5; see online ESI†). The value of zeta-potential, which is above ±30 mV demonstrates moderate stability against aggregation in terms of charge stabilization. As presented in Fig. 5, the peak absorption of the silver seeds was at 400 nm, while the peak absorption of the gold nanostars was between 600 nm to 850 nm, attributed to the plasmon modes associated with the core and tips of the nanostars.

Electrochemical characterization of the engineered DNA based sensor

The electrochemical behavior of each step of the DNA sensor fabrication was evaluated by CV technique in the presence of 0.01 M $(Fe(CN)_6)^{3/4}$–KCl) redox indicator. As shown in Fig. 6, the lowest peak current corresponds to the Au electrode. The peak from GNSs modified Au electrode confirms the deposition of the nanomaterial. The recorded high peak current for the GNSs/pDNA/MCE/TB Au electrode is attributed to the electroactivity of TB showing a high signal intensity. Enhancement of the current intensity after deposition of all corresponding modifying layers and hybridization of pDNA with tDNA compared with AuNSs modified gold electrode is evident. This phenomenon is associated with the effective surface area of the nanomaterial, loading a high number of sequences and the absorption effect of TB. The nature of the peak at around −0.7 is due to the interaction of labeled (TB) pDNA with cDNA sequences, confirming the successful hybridization in the presence of an electroactive agent. It should be pointed out that in label-free genosensors, there is no similar peak.

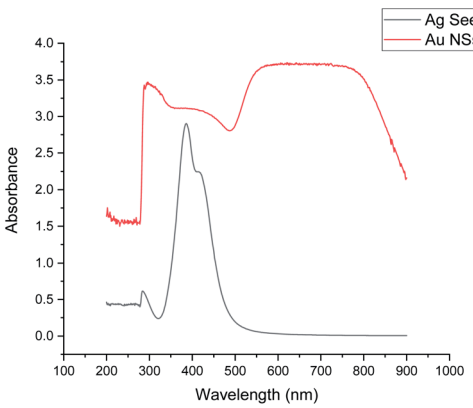

Fig. 5 UV-vis absorption spectra of silver seeds (black) and gold nanostars (red).

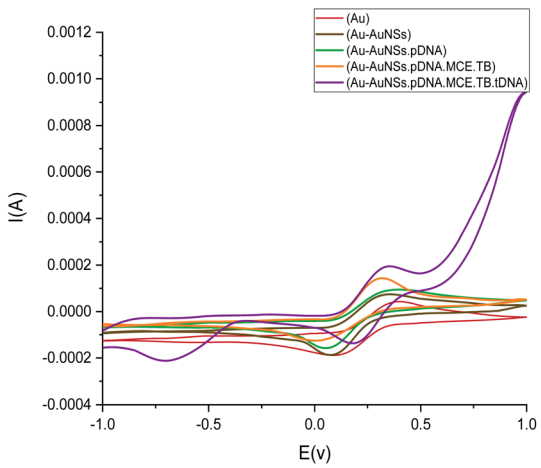

Fig. 6 CVs of the Au electrode, GNS-modified Au electrode, GNSs/pDNA/Au electrode, GNSs/pDNA/MCE/TBAu electrode, and GNSs/pDNA/MCE/TB/tDNA/Au electrode. Supporting electrolyte is 0.01 M $(Fe(CN)_6)^{3/4}$–KCl).

Optimization of the duration of DNA hybridization

DNA hybridization is considered as a rate-limiting step, which determines the *in situ* assay time. Optimization of the hybridization time was performed simply by immobilizing 5 μM of target DNA on the sensor with different incubation times (10, 30, and 40 min) at room temperature. SWV technique was adopted to record the response for each adjusted time of hybridization in the presence of 0.01 M $(Fe(CN)_6)^{3/4}$–KCl). (Fig. S6; see online ESI†) depicts the SWV response for each hybridization time. The DNA sensor exhibited a higher SWV response as the hybridization time was taken for 30 min. Therefore, 30 min was selected as the optimum time for hybridization of the probe DNA with target DNA in all steps of this study.

Selectivity study

The selectivity of the fabricated DNA sensor was determined using the probe DNA by allowing the hybridization process with complementary target DNA and mismatch sequences such as one-base mismatched DNA, two-bases mismatched DNA, and three-bases mismatched DNA on the genosensor for 30 min incubation time at room temperature. SWV technique was carried out to characterize the selectivity in the presence of 0.01 M $(Fe(CN)_6)^{3/4}$–KCl). The result and changes in the SWV plots are shown in (Fig. S7; see online ESI†). Hybridization with the target DNA resulted in a noticeable decrease in the current response in comparison with mismatch sequences. Upon hybridization with mismatch sequences, the current showed a change and increased, confirming the inappropriate hybridization with non-complementary sequences, which could be attributed to the mismatch bases. The intensity signal for three-base mismatched DNA exceeded the sequences with one and two mismatch bases, which demonstrates that the complete hybridization process failed and the increase in the current is due to the partial hybridization of the probe and non-complementary DNA, confirming the selectivity of the probe towards the target DNA.

Kinetic study

Cyclic voltammetry was adopted to evaluate the electrocatalytic behavior of the Au/GNSs electrode towards the redox

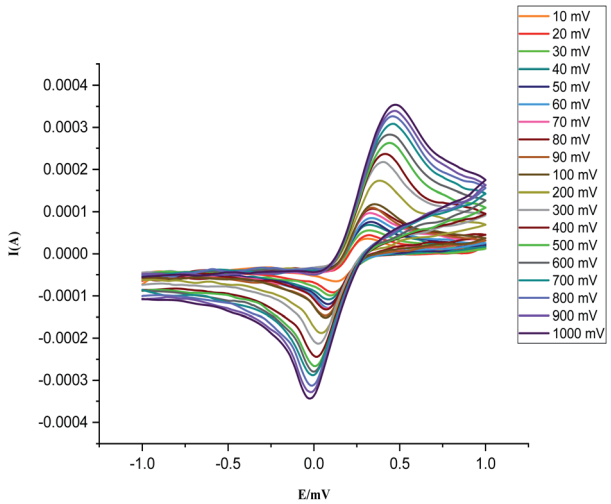

Fig. 7 CVs of Au/GNSs in 0.01 M $(Fe(CN)_6)^{3/4}$–KCl) in different potential sweep rates (from inner to outer): 10, 20, 30, 40, 50, 60, 70, 80, 90, 100, 200, 300, 400, 500, 600, 700, 800, 900, and 1000 mV s^{-1}.

behavior of $(Fe(CN)_6)^{3/4}$–KCl). The result of the CV as the function of scan rate for the Au/GNSs electrode is presented in (Fig. 7 and S8(A–E); see online ESI†). The anodic and cathodic peaks correlate to the oxidation and reduction of the $(Fe(CN)_6)^{3/4}$–KCl) redox couple. The anodic and cathodic peak currents were found to increase linearly with different potential sweep rates in the range of 10 to 1000 mV s^{-1}, confirming the diffusion-limited behavior of the electrochemical reaction of the redox couple. It could be deduced that in the slower scan rates, the electron exchange is slower on the electrode surface to record peak currents, resulting in narrower voltammograms with shorter current peaks. According to the linear dependency of the peak current *versus* the square root of the scan rate and Napierian logarithm of peak current *versus* Napierian logarithm of the scan rate (Fig. S8(B and C); see online ESI†), it could be inferred that the reaction is diffusion controlled. Accordingly, it could be stated that the electrochemical reaction and current density follow the well-known Randles–Sevcik equation.[31]

$$I_p = 269\,000AD^{1/2}n^{3/2}v^{1/2}C, \quad (1)$$

where I_p is the peak current, n is the number of transferred electrons ($n = 1$), A, the electroactive surface area (0.176 cm^2), D is diffusion coefficient, v is the scan rate, and C is the concentration of electrolyte. Moreover, the redox peak potential increased relatively with the scan rate, demonstrating the irreversible nature of the electrocatalytic property of the sensor. Additionally, the calculated slope of 0.5 (Fig. S8(C); see online ESI†) indicates that the process is diffusion controlled[32] (Fig. S8(E); see online ESI†). Indicates that in the higher scan rates, the redox pair reaction is reversible and in the slower scan rates, it is irreversible. The result of the kinetic study confirms the increased efficiency of Au/GNSs and its applicability in water-based electrochemical reactions.

Regeneration and interday stability study

The regeneration performance of the fabricated DNA sensor is presented in (Fig. S9; see online ESI†). To investigate the regeneration performance, after hybridization with 5 μM of target DNA, the sensor was kept at 60 °C for 4 min for dehybridization. Next, 5 μM of the same target DNA was drop casted for re-hybridization of the DNA sensor. As shown in (Fig. S9; see online ESI†), the SWV response of the sensor was regenerable, showing a slight decrease in the range of 6.9% compared to the initial response.

The interday stability (storage stability) of the Au/GNSs/pDNA electrode was assessed by comparing the electrochemical performance of the freshly prepared one with the stored electrode over 4 days at 4 °C. The result (Fig. S10; see online ESI†) indicated that the electrochemical response was preserved up to 3 days. Later, a significant increase in signal intensity was recorded, which might be attributed to the surface contamination of the electrode. The result confirmed that the electrode was stable for 72 hours.

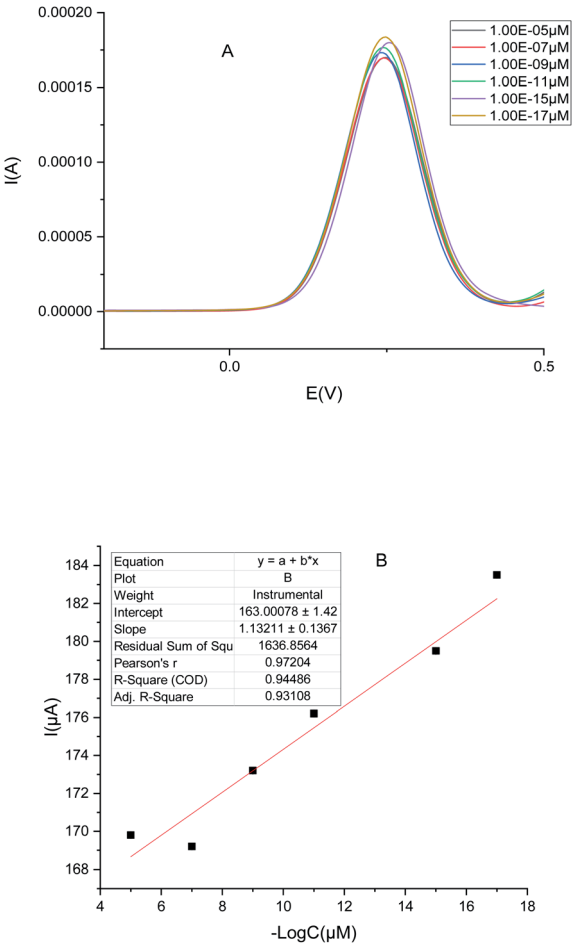

Fig. 8 (A) SWVs of the GNSs/pDNA/MCE/TBAu electrode for the detection of different concentrations of target DNA (AAC AAT GGG TCA GCG GTA AGG CTA) from 10^{-5} to 10^{-17} μM in 0.01 M $(Fe(CN)_6)^{3/4}$–KCl) with a pulse size of 100 mV. (B) Corresponding calibration curve. Error bars represent the standard deviation of time of the hybridization process ($n = 3$ per sample). Errors are less than a certain value.

Electrochemical response study of the genosensor

The electrochemical activity of the fabricated genosensor was analyzed at different concentrations of tDNA (from 10^{-5} to 10^{-17} μM) using the SWV technique with a scan rate of 0.1 V s^{-1}. The Au/GNSs/pDNA/MCE/TB electrode was applied to detect different concentrations of target DNA. The result of SWV voltammograms are presented in Fig. 8(A). Findings confirmed that the oxidation current was linear with the logarithmic plot of the different concentrations of the target DNA (Fig. 8(B)). The low limit of quantification for standard samples was found to be 10^{-17} μM. The findings confirm the effectiveness of the fabricated DNA biosensor, for biosensing applications by targeting specific DNA markers.

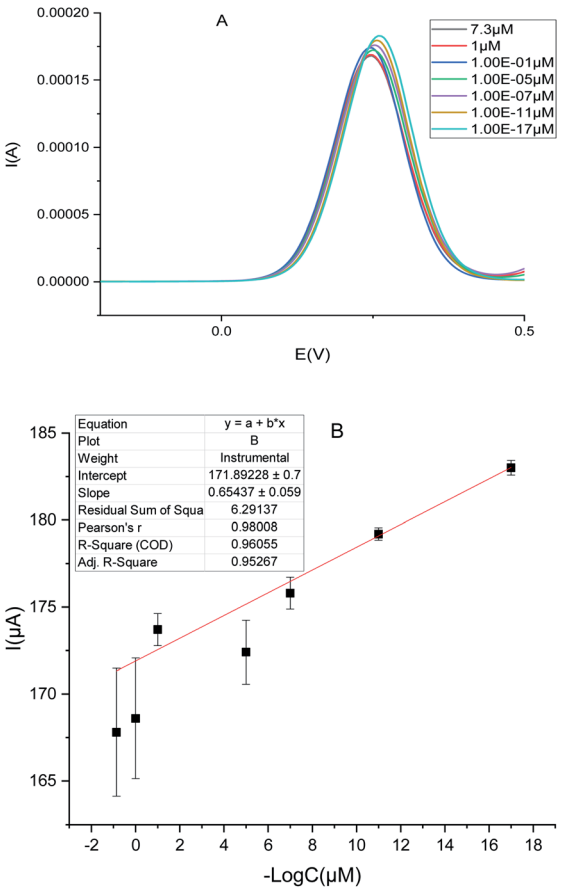

Fig. 9 (A) SWVs of the GNSs/pDNA/MCE/TBAu electrode for the detection of different concentrations of target DNA (AAC AAT GGG TCA GCG GTA AGG CTA) from 7.3 μM to 10^{-17} μM in 0.01 M $(Fe(CN)_6^{3/4}$–KCl) with a pulse size of 100 mV. (B) Corresponding calibration curve of different concentrations (from 7.3 to 10^{-17} μM). Error bars represent the standard deviation of the mean (reusability of the same electrodes).

E. coli detection from environmental samples

To evaluate the accuracy of the engineered DNA sensor, it was applied to detect the presence of *E. coli* in environmental water samples. Water samples were collected from the Motala river and used without any filtration. Samples were spiked with various amounts of target DNA for the detection of *E. coli* DNA. Fig. 9(A) shows the result of SWV voltammograms of different concentrations from 7.3 to 10^{-17} μM. Based on the corresponding calibration curve (Fig. 9(B)), the current was linear with the logarithmic plot of different concentrations in the range of 7.3 to 10^{-17} μM with LLOQ of 10^{-17} μM. Error bars represent the standard deviation of the mean (reusability of the same electrodes). Compared with other previously reported DNA assays based on different nanomaterials for the detection of *E. coli* O157:H7 (Table 2), the result confirms that the developed method based on gold nanostars has improved sensitivity and has the potential for detection of targeted bacteria in water samples. As summarized in Table 2, different nanomaterials and detection methods have been used for the construction of electrochemical genosensors to detect *E. coli* O157:H7. Despite the potential application of these nanomaterials, sensitivity, dissolution at high pH, and integration of expensive polymer for increasing the biosensing properties are the main drawbacks.[33,34] Anisotropic GNSs provide extraordinary biosensing platforms owing to their unique optical and electronic features, high surface-to-volume ratio, conductivity, catalytic properties, biocompatibility, low toxicity, and the ability for immobilization and high load of biological molecules like DNA while maintaining their properties.[35,36] According to Table 2, various detection techniques have been used to identify the target sequence of *E. coli* O157:H7. EIS provides information on the capacitance of the system and kinetics of multiple electrochemical processes. Sensitivity and nonspecific changes, which could be included in the signal, are some of the disadvantages of the EIS technique, which need to be considered.[37,38] In the present study, we used the SWV technique to detect the targeted sequence as it is one of the most sensitive and fastest pulse voltammetry techniques. SWV can perform the experiment faster than differential pulse voltammetry (DPV) due to the absence of background current leading to faster determination. This technique requires low consumption of the electroactive species. The detection limit by the SWV can be compared with those from spectroscopic and other chromatographic techniques.[39–41] The result of the present study indicates that the

Table 2 An overview of reported genosensors for the determination of *Escherichia coli* O157:H7

Type of nanomaterial	Detection method	Sample	Linear range (μM)	LOD (μM)	Ref.
ZnO nanorods/graphene nanoflakes	Impedimetric	Standard	1.0×10^{-10} to 1.0×10	1.0×10^{-11}	42
Graphene oxide/chitosan	EIS	Standard	1.0×10^{-8} to 1.0×10^{-2}	3.584×10^{-9}	43
Carbon dot/ZnO nano-road/PANI	DPV	Standard	1.3×10^{-12} to 5.2×10^{-6}	1.3×10^{-12}	44
Carbon nanotubes	DPV	Standard	1.94×10^{-7} to 2.01×10^{-8}	1.97×10^{-8}	45
Gold nanostars	SWV	Water sample	7.3 to 1.0×10^{-17}	1.0×10^{-17}	This work

application of GNSs leading to high load of the DNA along with the SWV technique for the first time provides fast and sensitive response for the target DNA sequence detection of *E. coli* O157:H7.

Conclusion

In recent years, there has been a noticeable increase in the integration of different nanostructures with sensors for the detection of pathogenic bacteria. Nucleic acids as the sensing elements pose an enormous potential for efficient detection of pathogenic bacteria. Intrinsic physicochemical stability of the genosensors makes them applicable in differentiating among different strains. Recent advances in nanotechnology have led to the integration of different nanomaterials into electrochemical DNA based biosensor construction to improve their sensitivity and performance. In summary, a rapid, sensitive, and specific electrochemical DNA biosensor was successfully designed for *E. coli* O157:H7 determination by targeting Z3276 specific genetic marker and employing gold nanostars for the first time. Stability, selectivity, and regeneration studies of the fabricated assay were carried out. The measurable electrochemical response of the hybridization reaction with the complementary target sequence, one-base mismatched DNA, two-base mismatched DNA, three-base mismatched DNA was measured *via* the SWV technique. The result indicated that the designed strategy could detect the complementary target sequence in a linear concentration range of 7.3 to 1×10^{-17} μM with a low limit of quantification of 0.01 zM in real water samples. Based on the result, deposition of the gold nanostars improved the sensitivity, specificity, and detection limit in samples without filtration. Findings showed that the proposed assay has potential application for the determination of *E. coli* O157:H7 in food safety and environmental monitoring purposes. Moreover, the fabricated strategy could be implemented as a promising format for other pathogenic bacteria detection. The high sensitivity of the sensing probe in the proposed study makes it practical to be commercialized and miniaturized as a hand-held device. Designing a strategy without employing tags for probe DNA and upstream processes with possible integration of phage-based technology could be promising steps towards commercialization of the strategy as a point of care device for water quality monitoring.

Funding

This research was funded by the European Union's Horizon 2020 research and innovation program under the Marie Skłodowska-Curie grant agreement No: H2020-MSCA-ITN-2018-813680.

Author contributions

Conceptualization, M. H. and N. R.; methodology, N. R.; software, N. R.; validation, M. H., O. N. and M. W.; formal analysis, N. R. and M. H.; resources, O. N. and M. W.; writing – original draft preparation, N. R.; review and editing, N. R., O.·N., M. H. and M. W.; supervision, M. W. and O. N.; funding acquisition, M. W. and O. N.; All authors have read and agreed to the published version of the manuscript.

Conflicts of interest

There are no conflicts to declare.

Acknowledgements

Authors gratefully acknowledge the financial support and funding from the European Union's Horizon 2020 research and innovation program under the Marie Skłodowska-Curie grant agreement No: H2020-MSCA-ITN-2018-813680.

References

1 E. Yuhana Ariffin, L. Y. Heng, L. L. Tan, N. H. Abd Karim and S. A. Hasbullah, *Sensors*, 2020, **20**, 1279.
2 Y. Zhang, C. Yan, H. Yang, J. Yu and H. Wei, *Food Chem.*, 2017, **234**, 332–338.
3 N. Razmi, M. Hasanzadeh, M. Willander and O. Nur, *Biosensors*, 2020, **10**, 54.
4 X. Cui, Y. Huang, J. Wang, L. Zhang, Y. Rong, W. Lai and T. Chen, *RSC Adv.*, 2015, **5**, 45092–45097.
5 L. W. Riley, R. S. Remis, S. D. Helgerson, H. B. McGee, J. G. Wells, B. R. Davis, R. J. Hebert, E. S. Olcott, L. M. Johnson and N. T. Hargrett, *N. Engl. J. Med.*, 1983, **308**, 681–685.
6 E. Y. Ariffin, Y. H. Lee, D. Futra, L. L. Tan, N. H. Abd Karim, N. N. N. Ibrahim and A. Ahmad, *Anal. Bioanal. Chem.*, 2018, **410**, 2363–2375.
7 W. Ye, T. Chen, Y. Mao, F. Tian, P. Sun and M. Yang, *Microchim. Acta*, 2017, **184**, 4835–4844.
8 I. G. Wilson, *Appl. Environ. Microbiol.*, 1997, **63**, 3741–3751.
9 Z. Shen, N. Hou, M. Jin, Z. Qiu, J. Wang, B. Zhang, X. Wang, J. Wang, D. Zhou and J. Li, *Gut Pathog.*, 2014, **6**, 1–8.
10 Z. Yu, G. Cai, R. Ren and D. Tang, *Analyst*, 2018, **143**, 2992–2996.
11 Z. Luo, L. Zhang, R. Zeng, L. Su and D. Tang, *Anal. Chem.*, 2018, **90**, 9568–9575.
12 L. Huang, J. Chen, Z. Yu and D. Tang, *Anal. Chem.*, 2020, **92**, 2809–2814.
13 Z. Yu, G. Cai, X. Liu and D. Tang, *Anal. Chem.*, 2021, **93**, 2916–2925.
14 R. Zeng, W. Wang, M. Chen, Q. Wan, C. Wang, D. Knopp and D. Tang, *Nano Energy*, 2021, **82**, 105711.
15 F. W. Scheller, F. Schubert, B. Neumann, D. Pfeiffer, R. Hintsche, I. Dransfeld, U. Wollenberger, R. Renneberg, A. Warsinke and G. Johansson, *Biosens. Bioelectron.*, 1991, **6**, 245–253.
16 S. Bansal, A. Jyoti, K. Mahato, P. Chandra and R. Prakash, *Electroanalysis*, 2017, **29**, 2665–2671.
17 T. E. Ouldridge, P. Šulc, F. Romano, J. P. Doye and A. A. Louis, *Nucleic Acids Res.*, 2013, **41**, 8886–8895.
18 A. Sassolas, B. D. Leca-Bouvier and L. J. Blum, *Chem. Rev.*, 2008, **108**, 109–139.

19 S. Ranallo, A. Porchetta and F. Ricci, *Anal. Chem.*, 2018, **91**, 44–59.
20 N. Shoaie, M. Forouzandeh and K. Omidfar, *Microchim. Acta*, 2018, **185**, 1–9.
21 L. Wu, E. Xiong, X. Zhang, X. Zhang and J. Chen, *Nano Today*, 2014, **9**, 197–211.
22 L. Qin, G. Zeng, C. Lai, D. Huang, P. Xu, C. Zhang, M. Cheng, X. Liu, S. Liu and B. Li, *Coord. Chem. Rev.*, 2018, **359**, 1–31.
23 M. e. T. Castañeda, S. Alegret and A. Merkoci, *Electroanalysis*, 2007, **19**, 743–753.
24 N. T. Perna, G. Plunkett, V. Burland, B. Mau, J. D. Glasner, D. J. Rose, G. F. Mayhew, P. S. Evans, J. Gregor and H. A. Kirkpatrick, *Nature*, 2001, **409**, 529–533.
25 R. Deshmukh, A. K. Prusty, U. Roy and S. Bhand, *Analyst*, 2020, **145**, 2267–2278.
26 B. Li and J.-Q. Chen, *Appl. Environ. Microbiol.*, 2012, **78**, 5297–5304.
27 Z. Kereselidze, V. H. Romero, X. G. Peralta and F. Santamaria, *J. Visualized Exp.*, 2012, **59**, e3570.
28 F. Bahavarnia, A. Mobed, M. Hasanzadeh, A. Saadati, S. Hassanpour and A. Mokhtarzadeh, *Enzyme Microb. Technol.*, 2020, **133**, 109466.
29 M. B. Haddada, J. Blanchard, S. Casale, J.-M. Krafft, A. Vallée, C. Méthivier and S. Boujday, *Gold Bull.*, 2013, **46**, 335–341.
30 N. A. Babu, L. Malathy and S. Mukherjee, *European Journal of Molecular & Clinical Medicine*, 2020, **7**, 749–756.
31 D. K. Gosser, *Cyclic Voltammetry: Simulation and Analysis of Reaction Mechanisms*, VCH New York, 1993.
32 A. J. Bard and L. R. Faulkner, *Electrochem. Methods*, 2001, **2**, 580–632.
33 A. Anand, U. Rajchakit and V. Sarojini, in *Nanomaterials for the Detection and Removal of Wastewater Pollutants*, Elsevier, 2020, pp. 69–110.
34 E. B. Bahadır and M. K. Sezgintürk, *TrAC, Trends Anal. Chem.*, 2016, **76**, 1–14.
35 S. M. Mousavi, M. Zarei, S. A. Hashemi, S. Ramakrishna, W.-H. Chiang, C. W. Lai and A. Gholami, *Drug Metab. Rev.*, 2020, **52**, 299–318.
36 G. Zhang, *Nanotechnol. Rev.*, 2013, **2**, 269–288.
37 A. Bogomolova, E. Komarova, K. Reber, T. Gerasimov, O. Yavuz, S. Bhatt and M. Aldissi, *Anal. Chem.*, 2009, **81**, 3944–3949.
38 A. Chamorro García, *Electrochemical and Optical Nanomaterial-Based Biosensors for Diagnostic Applications*, Universitat Autònoma de Barcelona, 2015.
39 V. Mirceski, S. Komorsky-Lovric and M. Lovric, *Square-wave Voltammetry: Theory and Application*, Springer Science & Business Media, 2007.
40 J. J. O'Dea, J. Osteryoung and R. A. Osteryoung, *Anal. Chem.*, 1981, **53**, 695–701.
41 J. G. Osteryoung and R. A. Osteryoung, *Anal. Chem.*, 1985, **57**, 101–110.
42 N. Jaiswal, C. M. Pandey, S. Solanki, I. Tiwari and B. D. Malhotra, *Microchim. Acta*, 2020, **187**, 1–8.
43 S. Xu, Y. Zhang, K. Dong, J. Wen, C. Zheng and S. Zhao, *Int. J. Electrochem. Sci.*, 2017, **12**, 3443–3458.
44 A. Pangajam, K. Theyagarajan and K. Dinakaran, *Sensing and Bio-Sensing Research*, 2020, **29**, 100317.
45 M. H. Abdalhai, A. n. M. Fernandes, X. Xia, A. Musa, J. Ji and X. Sun, *J. Agric. Food Chem.*, 2015, **63**, 5017–5025.